Electronic Journal of Structural Engineering



Original Article

Cite this: DOI: 10.56748/ejse.24796

Received Date: 28 March 2025 Accepted Date: 8 September 2025

1443-9255

https://ejsei.com/ejse

Copyright: © The Author(s). Published by Electronic Journals for Science and Engineering International (EJSEI). This is an open access article under the CC BY license. https://creativecommons.org/licenses/by/4.0/



Numerical Simulation Study on Dynamic Performance of Basalt Fiber Reinforced Polymer Anchor under Impact Load

Shaoyang Yan, Fuqiang Gao*, Pengli He, Jinjun Guo

- ^a School of Intelligent Construction and Civil Engineering, Luoyang Institute of Science and Technology, Luoyang 471023, China
- ^b Henan Key Laboratory of Green Building Materials Manufacturing and Intelligent Equipment, Luoyang 471023, China *Corresponding author: https://ligaofg@163.com

Abstract

The construction safety of underground structures, such as deep foundation pits, is seriously threatened under conditions of explosion vibration and underground water flow. The basalt fiber reinforced polymer (BFRP) anchor offers advantages such as light weight, high strength, strong corrosion resistance, good insulation, and cleanliness without pollution. It is widely used in mines, foundation pits, slopes, reservoir embankments, and other areas. To study the dynamic performance of BFRP anchors under impact loads, the LS-DYNA numerical simulation software was used to analyze the dynamic mechanical response of BFRP anchors under different impact loads and multiple impact load conditions. The research results indicate that: (1) The BFRP anchor can withstand energy impacts exceeding 2.5 kJ. At this level, the deformation of the BFRP anchor undergoes three stages: elastic deformation, plastic deformation, and elastic deformation rebound. (2) The stress and displacement of the BFRP anchor increase continuously with the rise in impact energy, with the highest stress and displacement values occurring at the joint. (3) The BFRP anchor can endure three impacts with an energy of 1.25 kJ. During the first and second impacts, the stress and strain initially increase and then decrease over time. However, during the third impact, the BFRP anchor fractures and fails, with stress and strain increasing continuously over time. The research results provide theoretical basis and reference for foundation pit support and slope anchoring y under dynamic load in special engineering geology.

Keywords

Impact load, Basalt fiber reinforced polymer anchor, Dynamic performance, Numerical simulation

1. Introduction

With the continuous improvement of China's comprehensive strength, the development of urban underground space has achieved rapid growth, and the depth of the foundation has also been continuously increased. However, During the construction process of deep foundation pits, support structure failure and seepage water are prone to occur, which are affected by dynamic loads such as underground dynamic water, blasting vibration, and seismic action (Jing et al. 2021, Bai et al. 2024). Compared with traditional reinforcement and support techniques, anchor bolt support offers advantages such as effective support, low economic cost, and ease of construction. It is widely used in engineering applications such as mines, foundation pits, slopes, and reservoir embankments (Fathollah and Mohsen 2019, Han et al. 2019). However, the corrosion of existing metal anchor rods is a significant issue due to long-term exposure to groundwater and corrosive media (Pirchio et al. 2023, Bujotzek et al. 2024). The fiber reinforced polymer (FRP) anchors are considered the best alternative to metal anchor rods due to their light weight, high strength, strong corrosion resistance, and excellent insulation properties (Zhao et al. 2020). Basalt fiber is a new type of inorganic, environmentally friendly, green and high-performance fiber material, which has stronger corrosion resistance and clean and pollution-free characteristics (Feng et al. 2024, Yan et al. 2020 and Zhao et al. 2024). The BFRP anchor can better coordinate the deformation of anchoring systems and have broad engineering application prospects.

In recent years, domestic and foreign scholars have conducted extensive research on the mechanical properties and anchoring characteristics of BFRP anchors based on laboratory tests and field tests. In terms of mechanical properties, Shi J.Z. et al. (Shi et al. 2015) conducted indoor experiments and theoretical analysis to investigate the effect of radial stress generated by anchoring components in the anchoring zone on the tensile properties of BFRP cables. Ren Y.H. et al. (Ren et al. 2024) studied the effects of pore size, anchorage length, and other factors on the anchoring performance and durability of basalt and glass hybrid fiberglass anchors under the synergistic action of freeze-thaw cycles and alkaline environments. Gu X.Y. et al. (Gu et al.2010) studied the basic mechanical properties of BFRP anchors with different diameters based on indoor experiments. The study found that the tensile elastic modulus of BFRP anchors decreased with increasing diameter. Xie J.Z. et al. (Xie et al. 2020) studied the mechanical behavior of BFRP anchors on joint surfaces using indoor anchor rock double shear tests. The study found that larger inclination angles or pre-tension can improve the shear bearing capacity of the connection surface and reduce relative displacement. Zhang S.B. et al. (Zhang et al. 2022) studied the anchoring shear performance of BFRP anchors and traditional steel reinforcement anchors in jointed rock layers. The study found that the BFRP anchors absorb significant amounts of energy, residual strength, and peak shear displacement before the shear peak. Zhao D.P. et al. (Zhao et al. 2021) studied the structural parameters of BFRP anchors and the critical anchorage length of BFRP cement mortar based on tunnel rock anchoring using mesoscale numerical simulations and laboratory experiments. Lin M.G. et al. (Lin and Lin 2023) investigated the effects of high temperature, freeze-thaw cycles on the mechanical properties such as strength and stiffness of BFRP anchor. The study found that the ultimate tensile strain decreases continuously with increasing temperature and freeze-thaw cycles. Wang L.P. et al. (Wang et al. 2019) studied the tensile, compressive, and shear mechanical properties of BFRP anchors under different acidic and alkaline corrosion environmental conditions. The study found that the tensile strength, compressive strength, shear strength and ultimate tensile strain of BFRP anchors all decreased in acidic and alkaline corrosion solutions. Wu G. et al. (Wu et al. 2014) conducted indoor long-term durability tests on BFRP anchors. Research has found that alkaline solutions have a higher impact on the durability of reinforcing materials than other solutions. Wang Z.K. et al. (Wang et al. 2017) used artificial accelerated aging tests to investigate the differences in durability between BFRP anchors and GFRP anchors exposed to seawater for a long time. The results showed that the alkali corrosion resistance of BFRP anchors was higher than that of GFRP anchors. In terms of anchoring characteristics. Motwani, P. et al. (Motwani et al. 2020) studied the anchoring slip of BFRP anchors under industrial anchoring using digital image correlation technology and linear potentiometers. Feng J. et al. (Feng et al. 2022) studied the influence of factors such as anchor type, diameter, and anchorage length on the bearing capacity and interfacial shear stress of anchors based on indoor testing. The research results showed that the pull-out load displacement curve of anchors showed a three-stage form, and the ultimate bearing capacity of anchors were proportional to the anchorage length and grouting diameter. Wang X. et al. (Wang et al. 2019) analyzed the bonding performance between BFRP bars and concrete from the perspectives of effective bond length, interface strain, and stress distribution. An analytical model for bond stress slip was established through data fitting. Shen D.J. et al. (Shen et al. 2019) conducted bond performance tests on BFRP bar concrete components with different strain rates. The law that the bond strength of BFRP bar reinforced concrete increases with the increase of strain rate and the slip decreases with the increase of strain rate has been elucidated. Zhu L. et al. (Zhu et al. 2017) preliminarily verified the applicability of BFRP

anchor rods through field tests on soil slope reinforcement. The recommended design parameters for BFRP anchor rod reinforcement of soil slopes have been determined, based on the comparison of the reinforcement effect of reinforced steel anchors. Feng J. et al. (Feng et al. 2019) conducted pull-out destructive tests on steel bar anchors and BFRP anchors of different diameters in loess areas. The anchoring characteristics of BFRP anchors have been studied. The results of indoor bonding tests and on-site static anchoring tests for BFRP anchors and other material anchors have been summarized. Research has shown that the engineering application performance of BFRP anchor is better.

Currently, most research is limited to static anchorage tests. There are few reports on the research of underground structural engineering using BFRP anchor under the influence of underground dynamic water, upper load transmission vibration, and earthquake. Therefore, it is crucial to study the mechanical properties of BFRP anchor under dynamic loads. However, it is challenging to observe structural changes in BFRP anchors during indoor dynamic load impact tests. In order to more clearly describe the stress and deformation characteristics of BFRP anchor under dynamic loads, LS-DYNA finite element numerical simulation software was used for related research. The results provide a theoretical basis and reference for foundation pit support and slope anchoring under dynamic loads in special engineering geology.

2. Methods

2.1 **Numerical Model Establishment of BFRP Anchor**

Based on the size parameters of BFRP anchors, a numerical model of BFRP anchors was established using CAD and CAE software. The numerical simulation and analysis flowchart of BFRP anchor is shown in Figure 1. As can be seen in Figure 1, the numerical modeling and analysis mainly include the following four steps:(1) The three-dimensional geometric model of BFRP anchor is established using SolidWorks software. (2) The mesh of the three-dimensional geometric model of BFRP anchor is divided using HyperMesh software. (3) The boundary conditions and initial impact load of BFRP anchor unit model are applied using LS-DYNA to simulate the dynamic impact process of BFRP anchor. (4) The numerical simulation results of BFRP anchor is analyzed using LS-Prepost post-processing software.

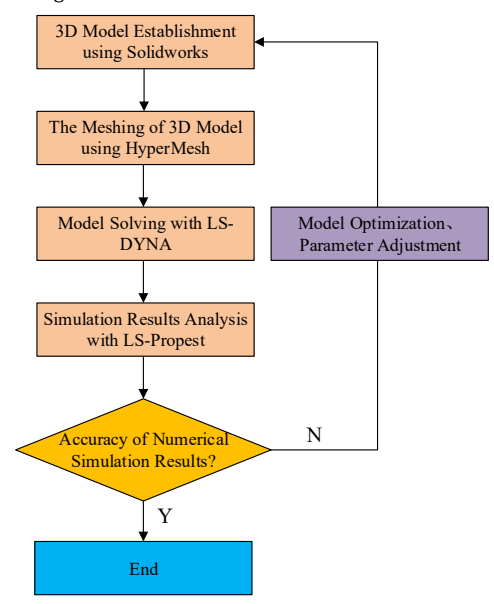
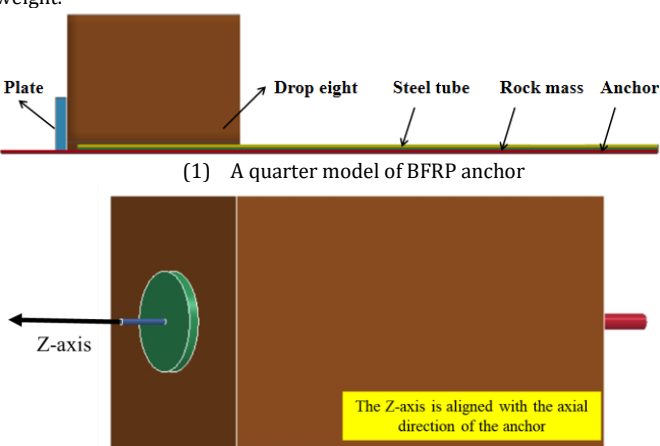


Fig. 1 The numerical simulation and analysis flowchart of BFRP anchor

The 3D geometric model of the BFRP anchor was created according to the process shown in Figure 1. However, the stirring module (3.0 cm long) in the BFRP anchor, which is only used to stir the resin, provides almost no anchorage force. Therefore, the stirring module of BFRP anchor is ignored for the convenience of geometric modeling. However, The BFRP anchor is composed of basalt fiber reinforcement, anchoring agents, plate, and other components. The final geometric length of the BFRP anchor is 120.0 cm, with an outer diameter of 12.4 mm. The plate is 108.0 cm away from the bottom. Outer diameter of the bonding layer is 20.0 mm. The outer diameter of the steel pipe is 32.0 mm. The drop weight used in the simulation is a rectangular mass with a centrally located circular hole. Due to this configuration and the symmetric geometry of the plate and anchor system, the impact force is expected to be approximately axisymmetric.

Table 1. The parameters of different model materials

Since the 3D geometric model is axisymmetric, a quarter 3D model of the anchor was established, and mesh generation was performed using HyperMesh. To verify the validity of using a quarter 3D model, we additionally developed a full 3D model without symmetry assumptions and compared the results. A total of 57,600 elements were generated for the anchor component, and the entire quarter model consists of 177,716 elements. The minimum element size in the anchor model is 5 mm. The mesh quality was carefully controlled, with the Jacobian value of all elements maintained below 0.7, ensuring high-quality mesh for reliable results. Established geometric model is shown in Figure 2, which consists of five parts: BFRP anchor, plate, steel tube, rock mass, resin, and drop weight.



(2) The full model of BFRP anchor

Fig. 2 Three-dimensional geometric model of BFRP anchor

2.2 **Constitutive Model and Material Parameters** of BFRP Anchor

The BFRP anchor primarily undergoes elastic-plastic deformation under dynamic impact conditions such as underground dynamic water, $upper\ load\ transmission\ vibration, and\ earth quake.\ Therefore, the\ bilinear$ elastic-plastic principal structure model was used for the BFRP anchor. The *MAT_PLASTIC_KINEMATIC model was chosen to describe the kinematic hardening plastic deformation of the material. The constitutive equation of the model is as follows:

$$\sigma_{y} = \sigma_{0} + \beta E_{p} \varepsilon_{eff}^{p}$$

$$E_{p} = \frac{E_{t}E}{E - E_{t}}$$
(2)

$$E_p = \frac{E_t E}{R_s R_s} \tag{2}$$

Where, σ_y is the yield stress; σ_θ is the initial yield stress; ε_{eff}^p is the effective plastic strain; E_p is the plastic hardening modulus; E is the elastic modulus; E_t is the tangent modulus.

Depending on the value of β , the material model can be divided into different hardening plasticity models. When β is equal to θ , the model is a kinematic hardening model; When β is equal to 1, the model is an isotropic hardening model. The kinematic and isotropic hardening models are shown in Figure 3.

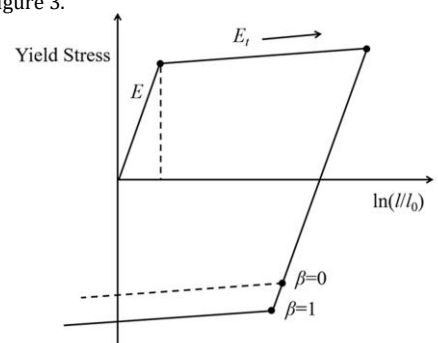


Fig. 3 Elastic-plastic models with kinematic and isotropic hardening

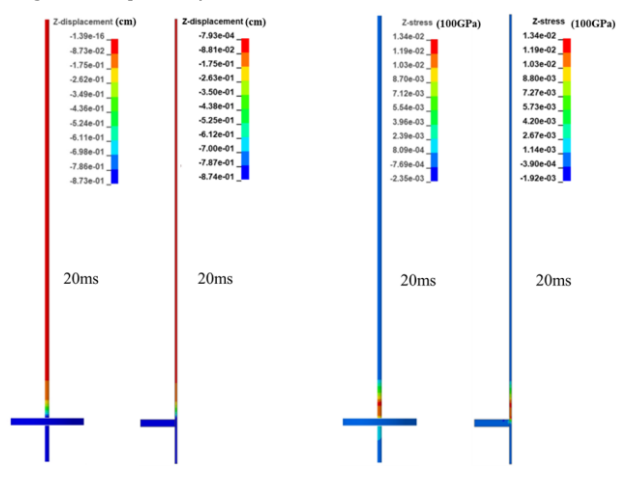
In addition, The *MAT_PLASTIC_KINEMATIC material model was selected for plate. The *MAT_SLASTIC_TITLE material model was selected for steel tube. The *MAT_SOIL_AND_FOAM material model was selected for resin. The *MAT_JOHNSON_HOLMQUIST_CONCRETE material model was selected for rock mass. The *MAT_RIGID material model was selected for drop weight. The specific material parameters of the model are shown in Table 1. The axial constraints were set at the end of the steel tube to prevent the steel tube from sliding. At the same time, different initial velocities were applied to the drop might to simulate different magnitudes of impact energy.

Material models	Parameter	Value	Parameter	Value	Parameter	Value
*MAT_PLASTIC_KINEMATIC	ro (g/cm³)	2.09	E (GPa)	48.45	$P_{ m r}$	0.27
	sigy (GPa)	0.0089	$\beta_{c}(GPa)$	5.60	beta	0.00
*MAT_ELASTIC_TITLE	ro (g/cm³)	7.83	E (GPa)	210.00	$P_{ m r}$	0.30
	da	0.00	db	0.00	/	/
*MAT_SOIL_AND_FOAM	ro (g/cm ³)	1.86	G (GPa)	6.39E-2	Bulk	0.30
	A_0	3.40E-13	A_1	7.03E-7	A_2	0.30
*MAT_JOHNSON_HOLMQUIST_CONCRETE	ro (g/cm ³)	2.60	G (GPa)	28.70	В	2.50
	N	0.79	f_{c} (MPa)	64.00	$f_{\rm t}$ (MPa)	6.5
*MAT_RIGID	ro (g/cm³)	7.85	E (GPa)	207.00	$P_{ m r}$	0.30
	N	0.00	Couple	0.00	Μ	0.00

2.3 Numerical Model Verification

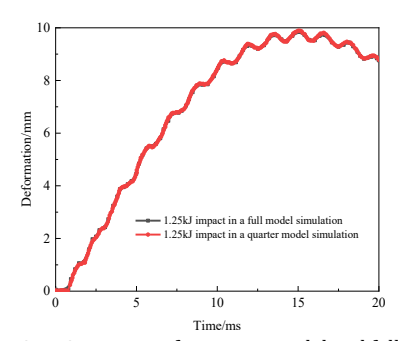
A Quarter Model and Full Model Result Analysis

To verify the validity of using a quarter 3D model of BFRP anchor, the deformation and stress of a quarter model and full model at 20 ms under 1.25 kJ were analyzed. Deformation cloud map and stress cloud map of a quarter model and full model of BFRP anchor under 1.25 kJ are shown in Figure 4, respectively. The deformation-time curve and stress-time curve of a quarter model and full model of BFRP anchor under 1.25 kJ are shown in Figure 5, respectively.

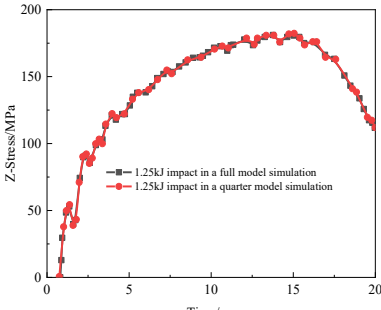


- (1) The deformation cloud map of a quarter model and full model of BFRP anchor
- (2) The stress cloud map of a quarter model and full model of BFRP anchor

Fig. 4 The deformation cloud map and stress cloud map of a quarter model and full model of BFRP anchor under 1.25 kJ



(1) The deformation-time curve of a quarter model and full model of BFRP anchor



(2) The stress-time curve of a quarter model and full model of $\ensuremath{\mathsf{BFRP}}$ anchor

Fig. 5 The deformation-time curve and stress-time curve of a quarter model and full model of BFRP anchor under 1.25 kJ

It can be seen from Figure 4 and figure 5 that the comparison shows that the deformation and stress distributions of the quarter model and the full model are in close agreement, confirming the reliability of the simplified model. Therefore, a quarter model is established to save the calculation time of the model in the subsequent simulation process.

Test and Simulation Result Analysis

The testing apparatus mainly consists of winches, fixture, drop weight, steel bar, a buffer device and other components as shown in Figure 6. The testing apparatus has a maximum power impact energy of 10 kJ, which can be controlled by adjusting the mass and height of the drop weight to regulate the magnitude of the impact energy. First, the crane lifts the drop weight to a certain height after the test specimen is mounted to the testing apparatus. Then, the drop weight is released to impact the test specimen.

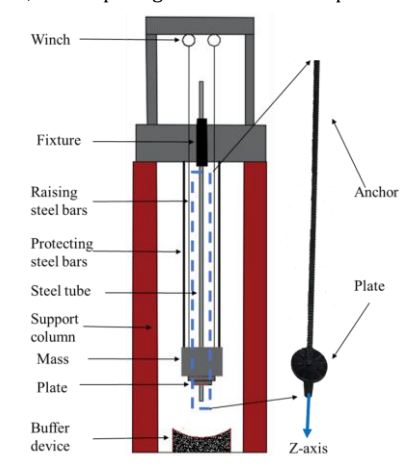


Fig. 6 Schematic diagram of dynamic impact testing device

In this test, the mass of the drop weight is 250 kg, and the crane lifts the drop weight to $0.5\,$ m. According to the gravitational potential energy formula E=mgh, the energy acting on the bolt is $1.25\,$ kJ. Steel tube is used to simulate rock mass in bolt impact tests. To quantitatively analyze the accuracy of the numerical simulation, the stress-time curve of BFRP anchor under $1.25\,$ kJ impact obtained by the tests and numerical simulation are plotted in Figure 4 for comparative analysis.

It can be seen from Figure 7 that the stress-time curve of BFRP anchor obtained by the numerical simulation is basically consistent with the test result, which are 182.38 MPa and 168.27 MPa, respectively. The stress-time curve of BFRP anchor obtained by simulation and test increases rapidly with time at first, then decreases gradually after reaching the peak value. The stress obtained from both numerical simulation and laboratory test are relatively small. This is consistent with the mechanical action mechanism of the BFRP anchor obtained from laboratory test. Based on the above analysis, it is considered reasonable to use the above material model and parameters for numerical simulation.

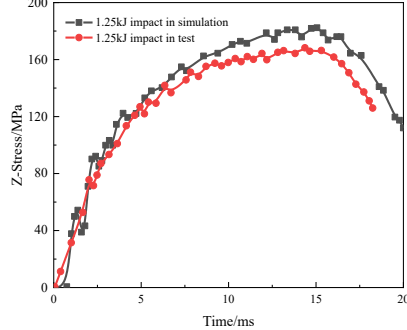


Fig. 7 Stress-time curve of BFRP anchor

3. Numerical Simulation Results and

Discussion

3.1 Different Impact Results and Discussion

Sometimes micro seismic events of different magnitudes occur due to blasting, underground water movement, etc., which results in different impact energies acting on the BFRP anchor. In order to study the dynamic characteristics of BFRP anchors under different impacts, four different impact energies of 1.25 kJ, 2.5 kJ, 5 kJ, and 10 kJ, were used to simulate the impact process of BFRP anchors.

Deformation Analysis and Discussion of BFRP Anchor under Different Impacts

The deformation cloud map and deformation-time curve of BFRP anchor under different impacts are shown in Figure 8 and Figure 9, respectively.

The conclusions drawn from Figure 8 and Figure 9 are as follows:

The deformation of the BFRP anchor increases continuously with the increase of impact energy. However, the deformation-time curves of the BFRP anchor under different energy impacts varies. When the impact energy is 1.25 kJ and 2.5 kJ, the deformation of the anchor first increases linearly, then the deformation growth rate slows down, and then the end deformation decreases. When it reaches a certain value, the deformation remains constant at the end. When the impact energy is 5 kJ and 10 kJ, the deformation time curve of the anchor is mainly a linear elastic line. In summary, when the impact energy is less than 5kJ, the anchor basically does not slip and undergoes elastic-plastic deformation internally. After a single impact, the deformation of the anchor undergoes an elastic retreat process. The final displacement of the anchor head at 1.25 kJ and 2.5 kJ is 8.30 mm and 16.20 mm, respectively. When the energy is 5 kJ and 10 kJ, the anchor only undergoes elastic-plastic deformation, and the final displacement is 19.95 mm and 25.20 mm. The anchor did not undergo elastic retreat, indicating that it broke and failed under impact energies of 5 kJ and 10 kJ. In addition, the duration of the impact process decreases as the impact energy increases. When the energy impact is 1.25 kJ and 2.5 kJ, the elastic-plastic deformation of the anchor reaches its maximum at 15.02 ms and 17.04 ms, respectively. When the impact energy is 5 kJ and 10 kJ, the entire process from deformation to failure of the anchor lasts for 10 ms and 8 ms, respectively.

Stress Analysis and Discussion of BFRP Anchor under Different Impacts

The stress cloud map and stress-time curve of BFRP anchor under different impacts are shown in Figure 10 and Figure 11, respectively. The conclusions drawn from Figure 10 and Figure 11 are as follows:

The stress of the anchor increases continuously with the increase of impact energy. However, the stress patterns under different energy impacts are similar. Under different energy impacts, the strain at the head of the anchor increases first. As the impact time increases, stress gradually transfers towards the anchoring end. When the impact energy is $1.25~\rm kJ$ and $2.5~\rm kJ$, the stress inside the anchor increases first and then decreases with time. When the impact energy is $5~\rm kJ$ and $10~\rm kJ$, the stress inside the anchor increases continuously with time. Until the anchor is destroyed, the stress instantly drops to $0.~\rm In~addition$, at the same time, the internal stress of anchors with lower impact energy is lower than that of anchors with higher impact energy.

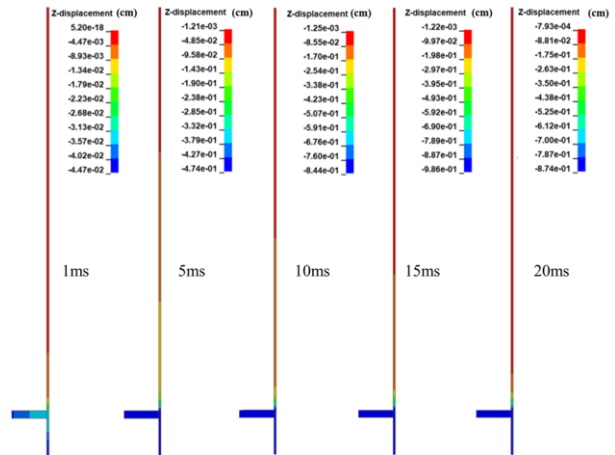
3.2 Multiple Impact Results and Discussion

Explosions and other dynamic loads occur frequently in engineering. In order to further investigate the mechanical properties of BFRP anchor under frequent dynamic loads. The repeated impact simulations were conducted on BFRP anchors using an energy of 1.25 kJ. The simulation results showed that under the action of 1.25 kJ impact energy, the BFRP anchor broke after the third impact.

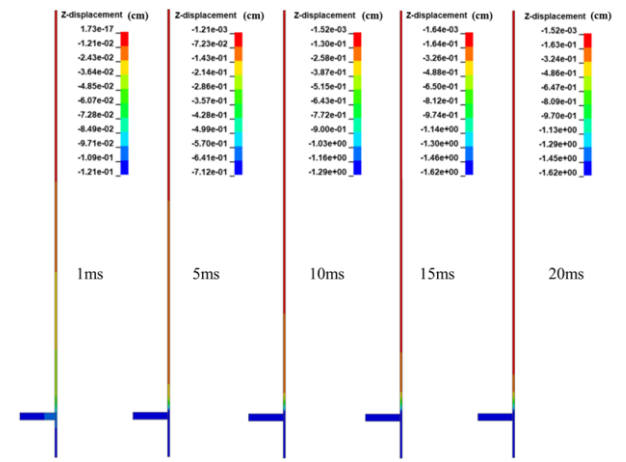
Deformation Analysis and Discussion of BFRP anchor under multiple impacts of 1.25 kJ $\,$

The deformation cloud map and deformation-time curve of BFRP anchor under multiple impacts of 1.25 kJ are shown in Figure 12 and Figure 13, respectively. The conclusions drawn from Figure 8(1) Figure 12 and Figure 13 are as follows:

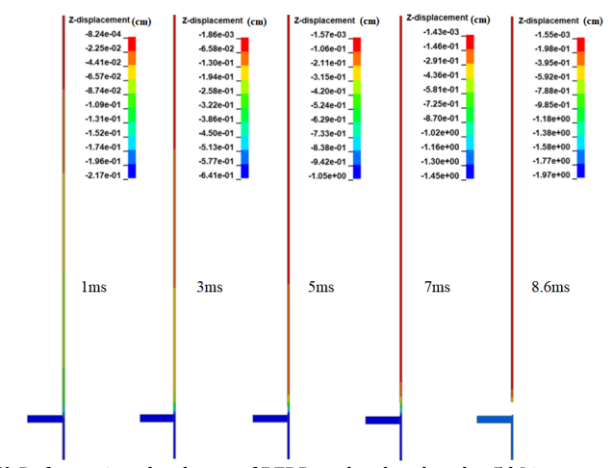
After three impacts with 1.25kJ on the BFRP anchor, the cumulative elongation of the anchor is 24.34 mm. The anchor underwent elastic-plastic deformation under both the first and second impacts of 1.25 kJ. The first deformation elongation of the anchor was greater than the second deformation elongation, which are 8.78 mm and 12.31 mm, respectively. However, under the second impact of 1.25 kJ, the anchor experienced significant sliding displacement. After the third impact of 1.25 kJ, the displacement of the anchor is linearly correlated with time, and there is no displacement rebound phenomenon. This indicates that the anchor fractured and failed under the third impact of 1.25kJ.



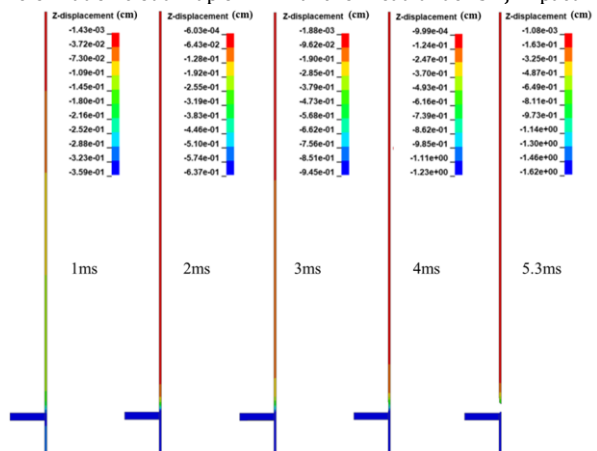
(1) Deformation cloud map of BFRP anchor under 1.25 kJ impact



(2) Deformation cloud map of BFRP anchor head under 2.5 kJ impact



(3) Deformation cloud map of BFRP anchor head under 5 kJ impact



(4) Deformation cloud map of BFRP anchor head under 10 kJ impact Fig. 8 The deformation cloud map of BFRP anchor under different

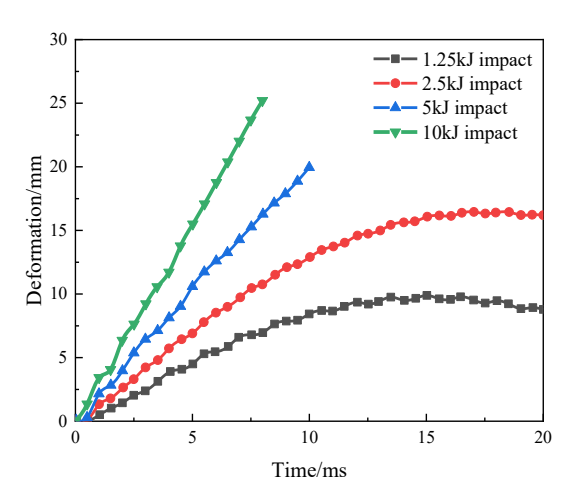
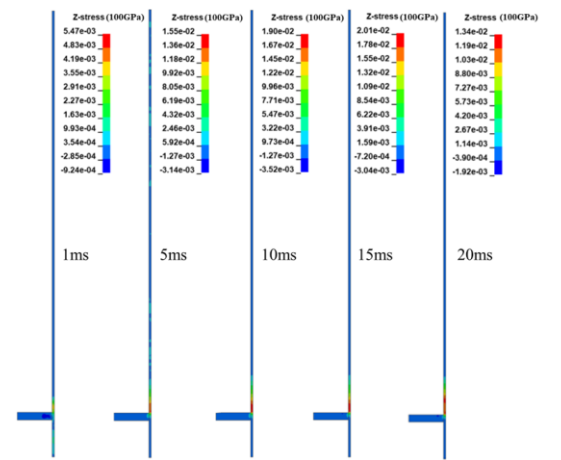
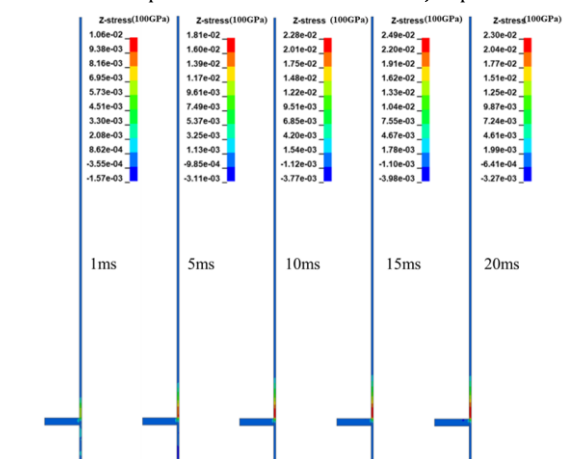


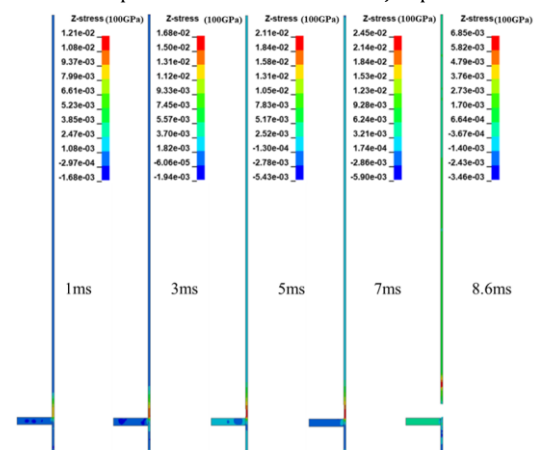
Fig. 9 The deformation-time curve of BFRP anchor under different impacts



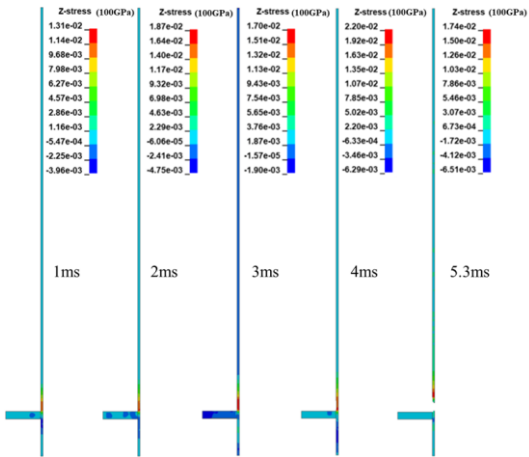
(1) Stress cloud map of BFRP anchor under 1.25 kJ impact



(2) Stress cloud map of BFRP anchor under 2.5 kJ impact



(3) Stress cloud map of BFRP anchor under 5 kJ impact



(4) Stress cloud map of BFRP anchor under 10 kJ impact

Fig. 10 The stress cloud map of BFRP anchor under different impacts

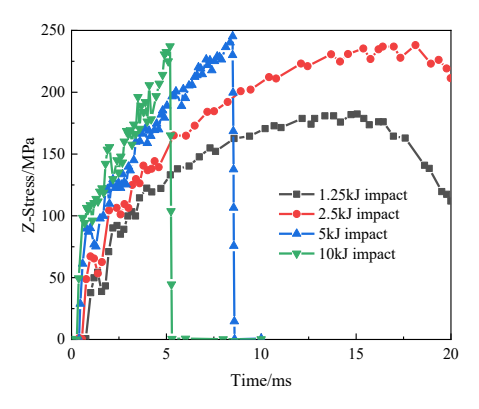
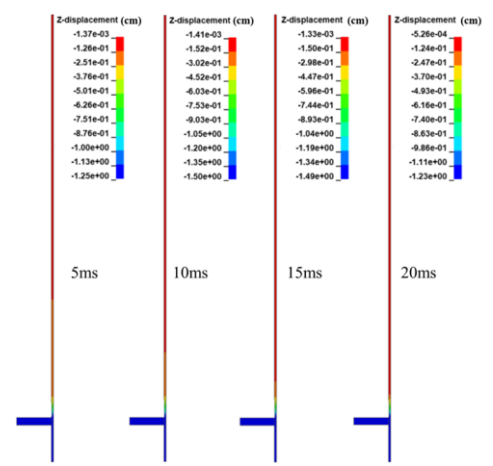
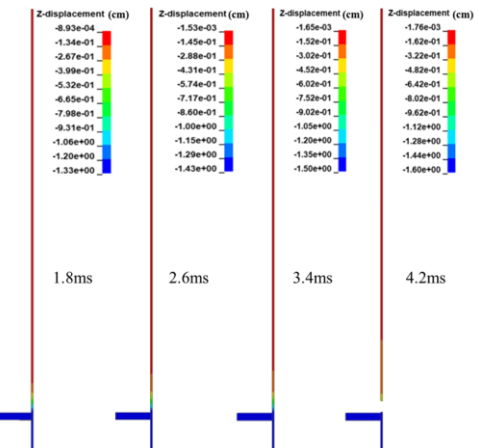


Fig. 11 The stress-time curve of BFRP anchor under different impacts



(1) The deformation cloud map of BFRP anchor under the second impact of 1.25 kJ



(2) The deformation cloud map of BFRP anchor under the third impact of

Fig. 12 The deformation cloud map of BFRP anchor under multiple impacts of 1.25 kJ

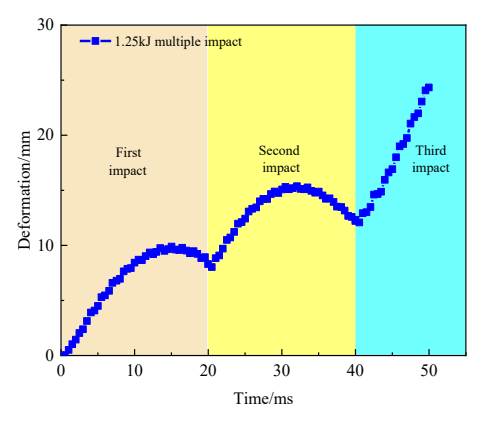


Fig. 13 The deformation-time curve of BFRP anchor under multiple impacts of 1.25 kJ

Stress Analysis and Discussion of BFRP anchor under multiple impacts of 1.25 kJ

The stress cloud map and stress-time curve of BFRP anchor under multiple impacts of 1.25 kJ are shown in Figure 14 and Figure 15, respectively.

The conclusions drawn from Figure 10(1) Figure 14 and Figure 15 are as follows:

The strain of BFRP anchor increases first and then decreases with time under both the first and second impacts of 1.25 kJ. Due to the direct fracture of the anchor after the third impact of 1.25 kJ, the strain of the anchor continued to increase with time. Until the anchor is destroyed, the stress instantly drops to 0. This is consistent with the variation pattern of anchor displacement. During the three impacts of 1.25 kJ, the strain at the anchor rod tray and the first anchoring module is relatively large. Therefore, compared to other positions of the anchor, the mechanical performance of the tray and the first anchoring module is significantly reduced. Due to the anchor radius at the tray being larger than the inner diameter of the first anchoring module, fracture and failure occurred first at the anchoring module.

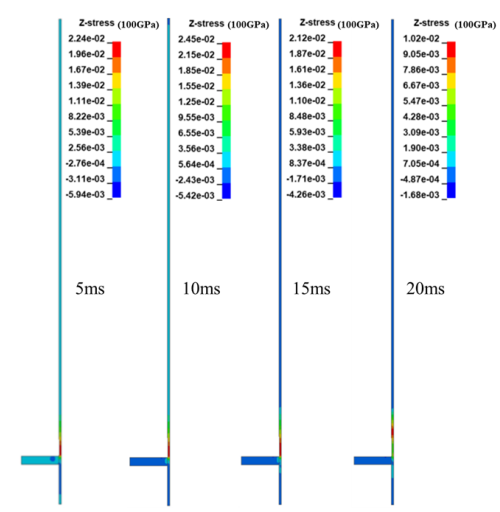
4. Conclusion

In this article, numerical simulation methods were adopted to study the dynamic performance of independently developed BFRP anchors under different impact energy levels and multiple impacts.

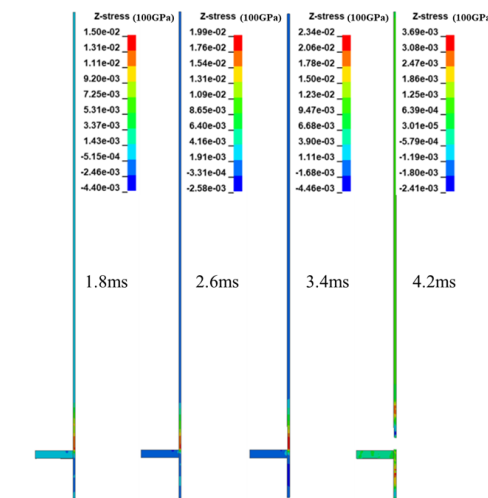
- (1) The BFRP anchor can withstand a single impact with an energy of 2.5 kJ. When the single impact energy is less than 2.5 kJ, the deformation of the anchor rod undergoes three stages: elastic deformation, plastic deformation, and elastic deformation rebound. When the single impact energy is greater than 5 kJ, the strain at the anchor plate increases, ultimately leading to fracture failure.
- (2) The displacement and internal stress of BFRP anchors increase with the increase of impact energy. When the impact energy is 1.25 kJ, 2.5 kJ, 5 kJ, and 10 kJ, respectively, the elongation of BFRP anchos is 8.78 mm, 16.20mm, 19.95mm, and 25.20mm. The maximum axial stresses of BFRP anchors are 182.37 MPa, 238.08 MPa, 245.29 MPa, and 237.16 MPa, respectively.
- (3) The total energy release capacity of BFRP anchor under multiple impacts reaches 3.75 kJ. After three impacts with 1.25kJ on the BFRP anchor, the cumulative elongation of the anchor is 24.34 mm. This indicates that BFRP anchors can resist dynamic impacts such as underground water and upper load transmission vibrations, while also reducing the damage to the anchors caused by dynamic impacts such as underground water and upper load transmission vibrations.

Acknowledgment

This study was supported by the Key Science and Technology Research Projects of Henan Province (No.252102320172) and the Natural Science Foundation of Henan Province (No.242300421255) and Key Research Projects of Higher Education Institutions in Henan Province (No.26B410003)



(1) The stress cloud map of BFRP anchor under the second impacts of 1.25 kg



(2) The stress cloud map of BFRP anchor under the third impacts of 1.25 kI

Fig. 14 The stress cloud map of BFRP anchor under multiple impacts of 1.25 kJ

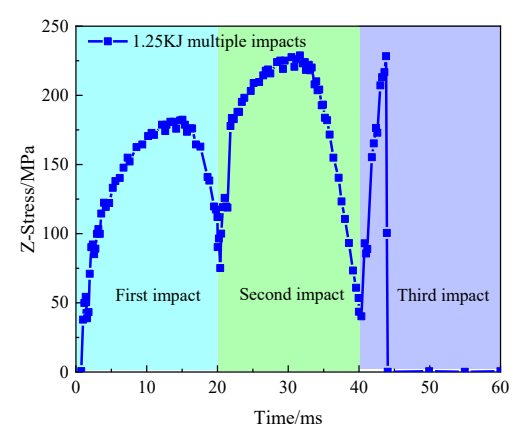


Fig. 15 The stress-time curve of BFRP anchor under multiple impacts of 1.25 kJ $\,$

References

Jing, D.S., Bai, X.Y., Feng, Z.W., Zhang, M.Y. and Li, C.C. (2021). "Feasibility Study of BFRP Anchor Used in Anti-floating of Underground Structure", Materials Reports, 35(19), 19223-19229. http://doi.org/10.11896/cldb.20080081

Bai, X.Y., Wu, Z.K., Wang, F.J., Sun, G., Zhang, M.Y. and Yan, N. (2024). "Load transfer behavior of BFRP anti-floating anchors based on field pull-out tests", Chinese Journal of Rock Mechanics and Engineering, 43(06), 1335-1346. http://doi.org/10.13722/j.cnki.jrme.2023.0898

Bujotzek, L., Beck, D., Apostolidi, E. and Waldmann, D. (2024). "Experimental and statistical investigations of the material properties of FRP reinforcement in compression", Construction and Building Materials, 414, 134782. http://doi.org/10.1016/j.conbuildmat.2023.134782

Fathollah, S. and Mohsen, S. (2019). "Evaluation and comparison of GFRP casing and CFRP sheets application on the behavior of circular

reinforced concrete column made of high-strength concrete", Asian journal of Civil Engineering, 20(8), 1153-1161. http://doi.org/10.1007/s42107-019-00172-8

Feng, G.Y., Guo, S.C., Zhou, L.L., Luo, W.H., Guo, X.K., Jin, Z.Q. and Zhu, D.J. (2024). "Effects of surface characteristics and alkalinity on the deterioration of BFRP bars and BFRP-SSC interface in seawater environment", Composites B-Engineering, 268, 111072. http://doi.org/10.1016/j.compositesb.2023.111072

Feng, J., Lai, B., Zhang, S.L., Wang, D. and Liu, Y. (2022). "Laboratory Pull-Out Test Study of Basalt Fiber Reinforced Polymer Bolt for Strengthening Mixed Soil", Journal of Southwest Jiaotong University, 57(06), 1193-1200.

Feng, J., Wang, Y., Wu, H.G., Lai, B. and Xie, X.D. (2019). "Field pullout tests of basalt fiber-reinforced polymer ground anchor", Rock and Soil Mechanics, 40(7), 2563-2573. http://doi.org/10.16285/j.rsm.2018.0552

Gu, X.Y., Shen, X. and Lu, J.Y. (2010). "Experimental Investigation on Tensile Mechanical Properties of BFRP Bars", Journal of Southwest Jiaotong University, 45(6), 914-919. http://doi.org/10.3969/Lissn.0258-2724.2010.06.016

Han, J., Zhang, M., Zhang, H.D., Tran, V.C., Cao, C., Ren, T. and Zhao, X.Z. (2019). "Rebar bolt optimization for large deformational roadways with application case", Journal of China University of Mining & Technology, 48(04), 727-734. http://doi.org/10.13247/j.cnki.jcumt.001028

Lin, M.G. and Lin, J.J. (2023). "Experimental Study on the Mechanical Properties of BFRP Bars after High temperature and Freeze-thaw Cycles", Journal of Railway Engineering Society, 40(08), 18-22.

Motwani, P., Perogamvros, N., Taylor, S. and Laskar, A. (2020). "Performance of industrial wedge-anchors for pre-stressing BFRP bars: Experimental and numerical studies", Composite Structures, 251, 112592. http://doi.org/10.1016/j.compstruct.2020.112592

Pirchio, D., Althouse, J.A., Madlem, T.A. Denavit, M.D., Weldon, B.D. and Walsh, K.Q. (2023). "Tensile strength and modulus of FRP pultruded composites at varying load anglesrelative to the pultrusion direction", Construction and Building Materials, 385, 131477. http://doi.org/10.1016/j.conbuildmat.2023.131477

Shen, D.J., Li, C.C., Feng, Z.Z., Wen, C.Y. and Ojha, B. (2019). "Influence of strain rate on bond behavior of concrete members reinforced with basalt fiber-reinforced polymer rebars", Construction and Building Materials, 228, 116755. http://doi.org/10.1016/j.conbuildmat.2019.116755

Shi, J.Z., Wang, X., Wu, Z.S. and Zhu, Z.G. (2015). "Effects of radial stress at anchor zone on tensile properties of basalt fiber-reinforced polymer tendons", Journal of Reinforced Plastics and Composites, 34(23), 1937-1949. http://doi.org/10.1177/0731684415606857

Ren, Y.H., Wang, H.G., Wu, G., Guan, Z.Z. and Yuan, L. (2024). "Study on the anchoring performance and failure mechanism of basalt/glass hybrid fiber reinforced plastic anchors in coupled environment", Polymer Composites, 45(1), 946-962. http://doi.org/10.1002/pc.27828

Wang, X., Su, C., Deng, W.J. and Wu, Z.S. (2019). "Bond behavior between corrugated BFRP shell and concrete under monotonic and cyclic loads", Construction and Building Materials, 210, 596-606. http://doi.org/10.1016/j.conbuildmat.2019.03.072

Wang, L.P., Zhang, C.T. and Li, B. (2019). "Effects of Acid-base Corrosion Environment on Mechanical Properties of BFRP Bars", Journal of Southwest University of Science and Technology, 34(02), 51-55.

Wang, Z.K., Zhao, X.L., Xian, G.J., Wu, G., Raman, R.K.S., Al-Saadi, S. and Haque, A. (2017). "Long-term durability of basalt- and glass-fibre reinforced polymer (BFRP/GFRP) bars in seawater and sea sand concrete environment", Construction and Building Materials, 139, 467-489. http://doi.org/10.1016/j.conbuildmat.2017.02.038

Wu, G., Zhu, Y., Dong, Z.Q., Wang, X. and Wu, Z.S. (2014). "Experimental study on the corrosion resistance performance of BFRP bars in the alkaline environment", China Civil Engineering Journal, 47(08), 32-41. http://doi.org/10.15951/j.tmgcxb

Xie, J.Z., Wang, X., Ding, L.N., Peng, Z.Q., Liu, X., Mao, W.Z. and Wu, Z.S. (2020). "Shear behavior of BFRP anchor-jointed rock mass considering inclination angle and pre-tension", Construction and Building Materials, 447, 138157. http://doi.org/10.1016/j.conbuildmat.2024.138157

Yan, S.Y., Jiao, H.Z., Yang, X.L., Wang, J.X. and Chen, F.B. (2020). "Bending Properties of Short-Cut Basalt Fiber Shotcrete in Deep Soft Rock Roadway", Advances in Civil Engineering, 2020(11), 1-9. http://doi.org/10.1155/2020/5749685

Zhao, J.F., Mei, K.H. and Wu, J. (2020). "Long-term mechanical properties of FRP tendon-anchor systems-A review", Construction and Building Materials, 230, 117017. http://doi.org/10.1016/j.conbuildmat..2019.117017

Zhao, D.P., Wen, S.X. and Zhu, L. (2024). "Dynamic characteristics of basalt fibre-reinforced polymer cement mortar bolts and its applicability for bolt defect detection", Journal of Building Engineering, 82, 108218. http://doi.org/10.1016/j.jobe.2023.108218

Zhao, D.P., Wen, S.X., Wang, L.W., Zhang, B.H. and Yang, L. (2021). "Structural parameters and critical anchorage length of tunnel system

bolts made of basalt fibre", Construction and Building Materials, 310, 125081. http://doi.org/10.1016/j.conbuildmat.2021.125081

Zhang, S.B., Wang, C.S., Wang, G., Wu, X.Z., Zheng, X., He, P. and Xu, F. (2022). "Experimental study on the shear behaviors of bolted rock joints reinforced with BFRP bars", Chinese Journal of Rock Mechanics and Engineering, 41(04), 712-724. http://doi.org/10.13722/j.cnki.jrme.2021.0894

Zhu, L., Kang, J.W., Zhao, W., Xie, Q. and Gao, X.J. (2017). "Experimental Study on Determining Design Parameters of Non-Prestressed BFRP Anchor for Supporting Soil Slope", Journal of Highway and Transportation Research and Development (English Edition), 11(4), 32-42. http://doi.org/10.1061/JHTRCQ.0000593

Disclaimer

The statements, opinions and data contained in all publications are solely those of the individual author(s) and contributor(s) and not of EJSEI and/or the editor(s). EJSEI and/or the editor(s) disclaim responsibility for any injury to people or property resulting from any ideas, methods, instructions or products referred to in the content.